

Dosimetry Effects Caused by Unilateral and Bilateral Hip Prostheses: A Monte Carlo Case Study in Megavoltage Photon Radiotherapy for Computed Tomography Data without Metal Artifacts

Courage Mahuvava, Frederik Carl Phillipus Du Plessis

Department of Medical Physics, Faculty of Health Sciences, University of the Free State, Bloemfontein, South Africa

Abstract

Background: Hip prostheses (HPs) are routinely used in hip augmentation to replace painful or dysfunctional hip joints. However, high-density and high-atomic-number (Z) inserts may cause dose perturbations in the target volume and interface regions. **Aim:** To evaluate the dosimetric influence of various HPs during megavoltage conformal radiotherapy (RT) of the prostate using Monte Carlo (MC) simulations. **Materials and Methods:** BEAMnrc and DOSXYZnrc MC user-codes were respectively used to simulate the linac head and to calculate 3D absorbed dose distributions in a computed tomography (CT)-based phantom. A novel technique was used to synthetically introduce HPs into the raw patient CT dataset. The prosthesis materials evaluated were stainless steel (SS316L), titanium (Ti6Al4V), and ultra-high-molecular-weight polyethylene (UHMWPE). Four, five, and six conformal photon fields of 6–20 MV were used. **Results:** The absorbed dose within and beyond metallic prostheses dropped significantly due to beam attenuation. For bilateral HPs, the target dose reduction ranged up to 23% and 17% for SS316L and Ti6Al4V, respectively. For unilateral HP, the respective dose reductions were 19% and 12%. Dose enhancement was always <1% for UHMWPE. The 6-field plan produced the best target coverage. Up to 38% dose increase was found at the bone–SS316L proximal interface. **Conclusions:** The novel technique used enabled the complete exclusion of metal artifacts in the CT dataset. High-energy plans with more oblique beams can help minimize dose attenuation through HPs. Shadowing and interface effects are density dependent and greatest for SS316L, while UHMWPE poses negligible dose perturbation.

Keywords: Dose perturbation, hip prostheses, Monte Carlo, radiotherapy, treatment planning

Received on: 14-07-2018

Review completed on: 24-10-2018

Accepted on: 24-10-2018

INTRODUCTION

Prostate cancer is one of the most frequently diagnosed male malignancies worldwide,^[1,2] with the majority of cases detected in men above 65 years old. This older population is furthermore affected by other age-related comorbidities such as osteoarthritis, for which a common treatment is prosthetic hip replacement. The number of hip replacements performed annually has increased from 210 per 100 000 males in 1998–1999 to 265 in 2006–2007.^[3,4]

High- Z prostheses cause dosimetric calculation errors when setting up a radiotherapy (RT) plan. This can be attributed to metal artifacts in the computed tomography (CT) dataset, which are perceived as starburst streaking and blurring

in kilovoltage CT images.^[5–7] Artifacts degrade the image diagnostic quality and impair contour delineation of target and critical organs.^[3,8] Several metal artifact reduction techniques have been implemented to partially compensate for CT artifacts.^[9–15]

Prostate cancer is often treated with brachytherapy and/or external beam RT (EBRT). EBRT strategies for prostate cancer include beam arrangements of 4, 5, 6, or more uniform beams,

Address for correspondence: Dr. Frederik Carl Phillipus Du Plessis,
Department of Medical Physics, Faculty of Health Sciences,
University of the Free State, P.O. Box 339, Bloemfontein 9300, South Africa.
E-mail: duplessisfcp@ufs.ac.za

This is an open access journal, and articles are distributed under the terms of the Creative Commons Attribution-NonCommercial-ShareAlike 4.0 License, which allows others to remix, tweak, and build upon the work non-commercially, as long as appropriate credit is given and the new creations are licensed under the identical terms.

For reprints contact: reprints@medknow.com

How to cite this article: Mahuvava C, Du Plessis FC. Dosimetry effects caused by unilateral and bilateral hip prostheses: A monte carlo case study in megavoltage photon radiotherapy for computed tomography data without metal artifacts. *J Med Phys* 2018;43:236–46.

Access this article online

Quick Response Code:



Website:
www.jmp.org.in

DOI:
10.4103/jmp.JMP_70_18

ranging from 6 to 18 MV.^[16,17] To reduce the dosimetric effects of hip prostheses (HPs), Eng^[18] suggested a 6-field (6F) conformal technique with high-energy photon beams, increasing the anterior–posterior/posterior–anterior (AP/PA) beam weighting in a conventional 4-field (4F) technique or using bilateral rotational arcs. Efforts have also been made to demonstrate the use of advanced RT techniques such as volumetric modulated arc therapy (VMAT).^[19] Dose conformity may be improved by intensity-modulated RT (IMRT) techniques.^[2,8,20]

The American Association of Physicists in Medicine: Radiation Therapy Committee Task Group 63 (AAPM TG-63) report^[21] advocates beam arrangements that avoid HPs in the beam's eye view. However, this approach restricts the choice of exploitable gantry angles, and the resultant dose distributions suffer from poor dosimetric conformity.^[21,22] Oblique beam orientation is further limited by its escalation of bladder and rectal tissue dose.

The concern is tumor dose reduction due to radiation attenuation through the HP and induced scattered dose near the prosthesis. These dose perturbations (radiation attenuation and scatter) may not be accurately predicted in conventional treatment planning systems (TPS), especially near tissue–bone–HP interfaces.^[23] Monte Carlo (MC)-based systems, on the other hand, can accurately quantify the dosimetric influence of HPs. The MC simulation accuracy is, however, limited by the accuracy of the density assignment performed using the CT dataset and is thus limited by the presence of artifacts.

This study evaluates the dose perturbation effect of SS316 L, Ti6Al4V, and UHMWPE HPs during high-energy conformal X-ray prostate treatment using MC simulations. The method used enables the complete exclusion of imaging artifacts by synthetically introducing the prosthesis into the femur of the raw patient CT data using a masking method.

MATERIALS AND METHODS

This study was approved by the University of the Free State Health Sciences Research Ethics Committee; reference number ECUFS NR 25/2015.

The MC technique used is a two-step process, simulating the linac head design and then simulating the dose distribution in a virtual phantom. BEAMnrc^[24] was used to build a 3D model of an Elekta Precise unit operating at three nominal photon energies of 6, 10, and 15 MV. The linac model was also modified to create a 20 MV virtual machine.

The accelerator head [Figure 1] was simulated based on the manufacturer's geometric and material specifications. The phase space data generated from BEAMnrc simulation was scored below the linac head exit window and contains all the information relating to the incident beam, e.g., particle energy, position, charge, and direction.^[25,26]

The second stage of the calculation involved using DOSXYZnrc^[17,27] to calculate the dose distribution in a CT phantom. DOSXYZnrc was also used to calculate the dose

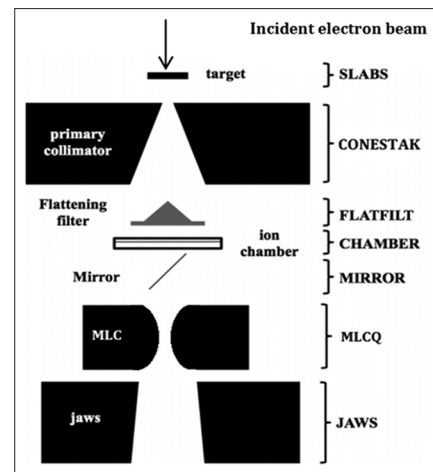


Figure 1: The geometry used for modeling the Elekta Precise linac head in BEAMnrc. The component modules used to simulate each linac component are shown on the right hand side

distribution in a homogenous water tank (WT) for linac beam characterization before CT-based simulations. The dose error associated with all simulations was kept below 1%.

Water tank simulations – photon beam characteristics

For analysis of photon beam characteristics, a 40 cm × 40 cm × 40 cm homogenous WT was simulated under the linac head at 100 cm source-to-surface distance. Voxels of size 0.2 cm × 0.2 cm × 0.2 cm were used. X-ray square fields of 5, 10, 15, and 20 cm per side and energies 6, 10, 15, and 20 MV incident perpendicularly on the WT were simulated. Central axis percentage depth dose (PDD) curves and dose profiles normalized to the depth of maximum dose (d_{max}) were presented.

Computed tomography-based simulations

A CT-based phantom from scanned patient images was used as the patient model. Generating a CT-based phantom with HPs was a two-step process, contouring the shape of the prosthesis into a raw pelvis CT dataset in MCSHOW graphical user interface (GUI) and then converting the mask media and density information into the desired HP using an IDL code. This is illustrated in Figure 2. The code reads in an *.*egs4phant* file, the phantom media, the media density data, as well as the mask (delineated HP volume) media data. The code then changes the mask media type into the HP media as well as the mask physical density into the physical density of the desired prosthesis material and write the output as a new phantom file.

MCSHOW allows for contouring, slice by slice, the shape of the HP, reproduced from a CT dataset of a patient with a HP, onto the actual patient CT dataset (*.*egs4phant* file) and substituting bony tissue with the prosthesis material. Unilateral and bilateral HP patient models were generated. The resulting phantoms were exported to DOSXYZnrc for dose calculations. The dose distribution data were stored in *.*3ddose* files from where PDD, dose-volume histogram (DVH), and dose profile data were extracted. CT-based profiles were normalized to the

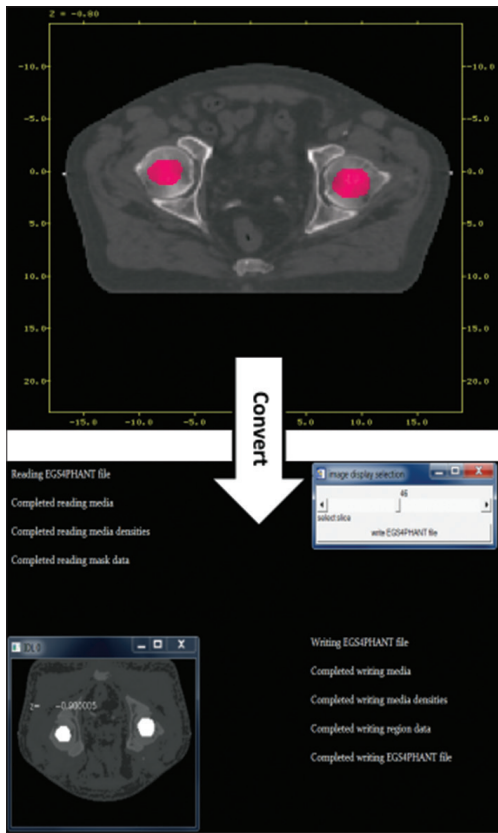


Figure 2: Illustration of the masking method. The top figure shows the transversal delineation of hip prostheses into the original computed tomography data using MCGSHOW and the bottom figure shows how the IDL code generates a phantom with hip prostheses and no artifacts by overriding the mask media data with hip prostheses data

isocenter dose with no HP. Since HPs were embedded into the CT dataset, the absorbed dose with and without HPs as well as dose perturbation factors were calculated in artifact-free CT phantoms. The specific PEGS4 cross-sectional data were calculated for each HP material in the EGSnrc Multi-platform (EGSnrcMP) GUI. The compositions of the HPs are shown in Table 1.^[21,28]

XiO TPS was used to define treatment beam portals for prostate three-dimensional conformal RT (3DCRT) to allow translation of the beam setup to DOSXYZnrc for phantom simulations. Beam setup (beam port configuration, beam size, and isocenter position) translation was performed using a set of transformation equations derived by Zhan *et al.*^[29]

The dosimetric impact of HPs was investigated on central axis PDDs, dose profiles, and DVHs of patient CT-based simulations. DVHs were used to compare the dose to the planning target volume (PTV) and to organs at risk (OARs). The back-scattered dose perturbation factor (BSDF) on the HP entrance side and the forward dose perturbation factor (FDPF) on the HP exit side were calculated as $BSDF \text{ (or FDPF)} = D_i/D_h$, where D_i and D_h are the respective doses at a point with and without the HP. The AAPM TG 105 recommendations^[30] were followed with respect to normalization, material conversion, and dose-to-material/dose-to-water calculations.

Table 1: The composition of titanium, stainless steel, and ultra-high-molecular-weight polyethylene used to generate implant PEGS4 cross-sectional data in Monte Carlo simulations

Implant material	Ti6Al4V	SS316L	UHMWPE
Mass density (ρ) (g/cm ³)	4.34	8.10	0.95
Effective atomic number (Z)	21.4	26.7	5.4
Composition (percentage by weight)	Ti: 89.947 Al: 5.80 V: 3.92 Fe: 0.18 O: 0.11 H: 0.012 C: 0.01 Y: 0.001	Fe: 63.70 Cr: 18.50 Ni: 12.00 Mo: 3.00 Mn: 2.00 Si: 0.75 P: 0.03 S: 0.03	H: 14.29 C: 85.71

Ti6Al4V: Titanium, SS316L: Stainless steel, UHMWPE: Ultra-high-molecular-weight polyethylene, PEGS4: Pre-processor for Electron Gamma Shower (version 4.0)

RESULTS

Water tank simulations – photon beam characteristics

For analysis of photon beam characteristics, simulated dosimetric parameters from PDD curves and dose profiles were compared with measured values from the machine’s commissioning data in a WT.

Dose profiles

Figure 3a-d present the simulated in-plane dose profiles (cross-plane profiles not shown) for the given range of beam energies and field sizes in a WT. An in-plane profile is defined as being along the beam data y-axis and a cross-plane profile is along the x-axis.

Percentage depth dose curves

Table 2 shows the simulated percentage doses at 10 cm depth ($PDD_{10\text{cm}}$) as well as d_{max} values in a WT. The simulated values shows good agreement ($\leq 1\%$) with measured values (in brackets) obtained from the Elekta Precise unit commissioning data.

Computed tomography-data based treatment planning and simulations

The prostate was delineated as the clinical target volume (CTV). OARs (the bladder and rectum) were also delineated to evaluate the dose to these organs which governs the use of fields through the prosthesis. The PTV was generated by a 1.0 cm isotropic expansion of the CTV (excluding seminal vesicles). The dose was delivered using 4-, 5-, and 6 equally-weighted, isocentric coplanar beams.^[21] The isocenter coordinates were positioned at the PTV centre for a supine, head-first patient setup. A dose of 75 Gy was prescribed to the PTV with $\geq 95\%$ of the prescription dose covering the PTV, based on the International Commission on Radiation Units and Measurements (ICRU) 50 guideline^[31] that stipulates that an optimal plan is one wherein the whole PTV receives between 95% and 107% of the prescription dose. Plans were compared for PTV coverage and the influence of increasing the number of beams from 6 to 20 MV. Interface effects were

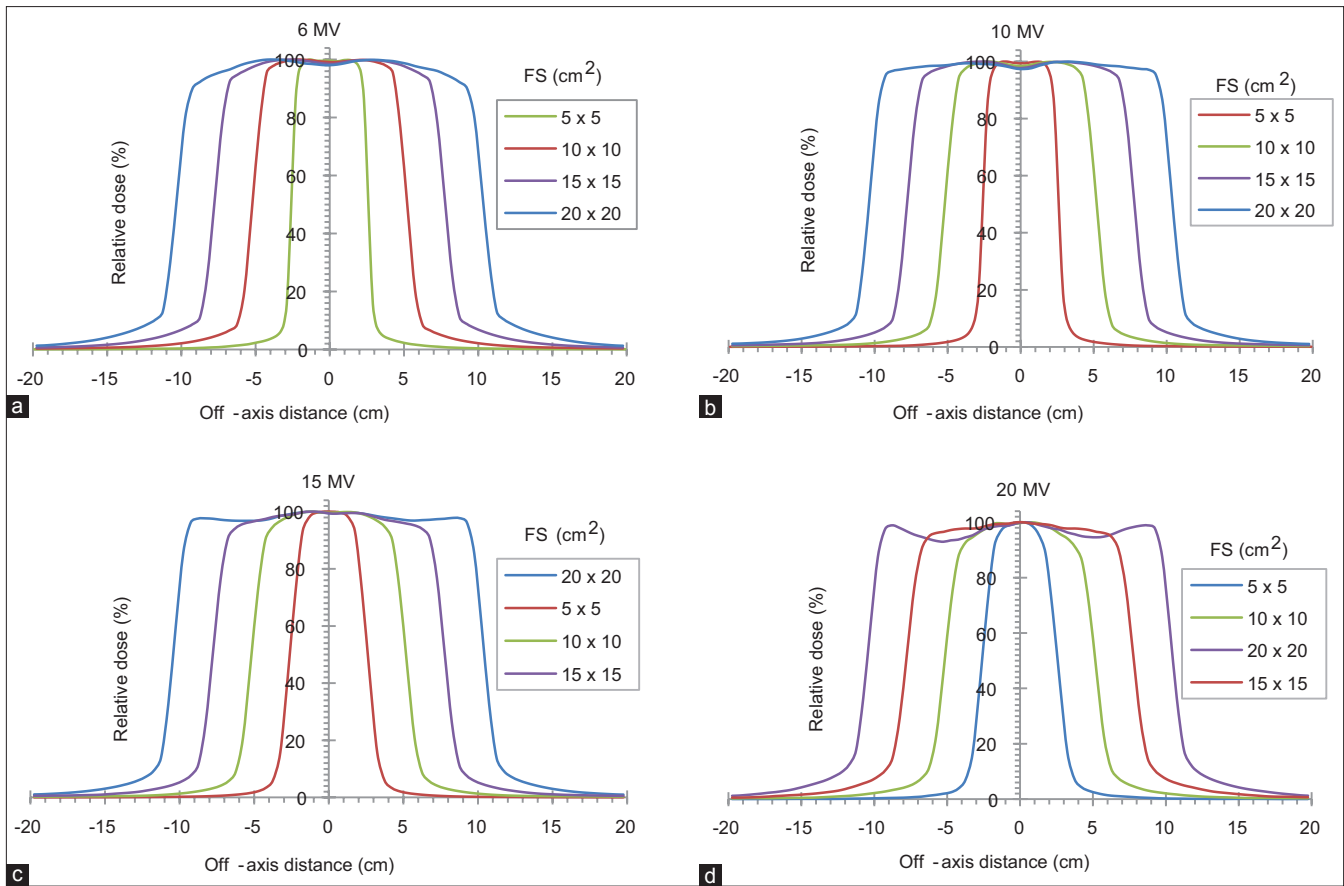


Figure 3: Simulated in-plane dose profiles for (a) 6 MV, (b) 10 MV, (c) 15 MV, and (d) 20 MV beams at various field sizes in water at 10 cm depth. The 20 MV data were simulated from a virtual linac

Table 2: Depth of maximum dose and percentage doses at 10 cm depth values for all field sizes and beam energies used

Energy (MV)	D_{max} (cm)	PDD _{10 cm} (%)			
		5×5 cm ²	10×10 cm ²	15×15 cm ²	20×20 cm ²
6	1.7 (1.7)	63.7	67.3 (67.9)	70	70.2
10	2.5 (2.5)	71.6	73.8 (73.3)	74.3	75.2
15	2.9 (3.0)	75	76.5 (75.9)	77.8	77.9
20	3.5 (-)	81.9	82.6 (-)	83.8	83.8

D_{max} : Depth of maximum dose, PDD_{10 cm}: Percentage doses at 10 cm depth

also evaluated on lateral dose profiles intersecting the implant. The beams were forced to intercept the prostheses because the aim was to evaluate the attenuation effect of prostheses during complete HP irradiation. The data are presented in such a way as to show under- or overdosage if the prosthesis is not accounted for.

Four-field box plan

The planar isodose distributions of the 4F plan with opposing bilateral and AP/PA beams in three different scenarios is presented in Figure 4a-c.

The effect of various bilateral HPs on the DVH data for the PTV, bladder, and rectum using this technique is shown in Figure 5a-d.

Maximum PTV dose perturbation occurs for SS316L, followed by Ti6Al4V, and then UHMWPE. The target coverage was quantified by comparing the PTV receiving at least 95% of the prescribed dose ($V_{95\%}$). In the presence of bilateral SS316L HPs, up to 89.5% of the PTV is underdosed at 6 MV, which reduces to 53.5% at 20 MV. This underdosage can be compensated for using higher AP/PA beam weights.^[18,26] The underdosed volume for a patient with Ti6Al4V ranges from 75.8% to 14.2%. No underdosage occurred for UHMWPE. To evaluate the dose-volume effect to OARs, the rectal and bladder volume receiving at $\geq 80\%$ of the prescription dose ($V_{80\%}$) was calculated. The maximum $V_{80\%}$ (or V_{60Gy}) value for the rectum and bladder in this 4F plan is 16% and 27%, respectively.

Local dose perturbations (interface effects) also occur in the vicinity of HPs. The “horns” in Figure 6 are due to electron backscatter from metallic HP surface on the proximal interface, relative to the lateral beam direction.

This effect was absent for UHMWPE, which showed a profile close to the one without HPs. The peak local hot spot due to backscattered electrons from SS316L was about the same as the PTV dose. This was for a patient ~36 cm in diameter in the lateral direction. Thus, the interface dose can be as high as the PTV dose. The BSDF at distance P from the proximal

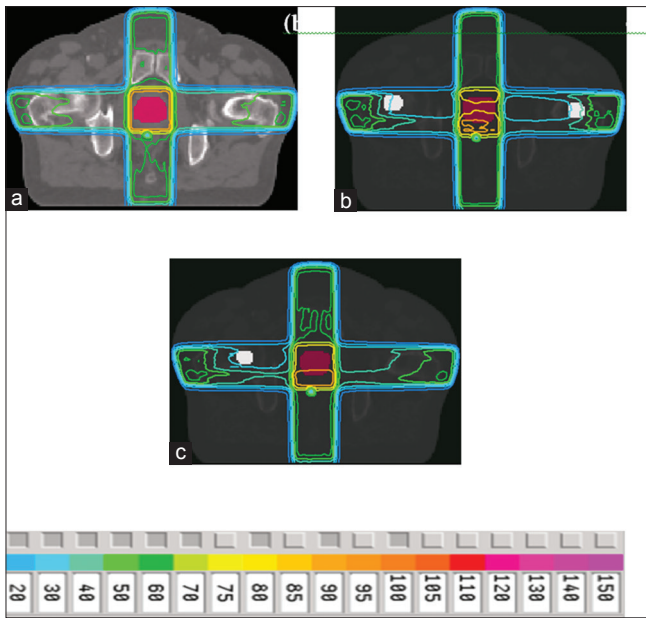


Figure 4: Transverse isodose distributions and isodose levels of a 4-field box for a patient with (a) no hip prostheses, (b) a bilateral SS316L, and (c) unilateral SS316L. The planning target volume is shown as the region intersected by the beams

interface is presented in Table 3a-d. Backscatter radiation at 6 MV contributed a small peak extending ~5 mm, which is the order of the range of secondary electrons scattered from the SS316L surface. For 10, 15, and 20 MV beams, backscatter perturbation extended ~0.9 cm, 1.2 cm, and 1.5 cm from the HP, respectively. Up to 38% local dose increase was observed at the bone–SS316L proximal boundary.

The change in the disequilibrium magnitude at the exit interface was quantified by the FDPF as presented in Table 4a and comparison was made with the FDPF values from Reft *et al.*^[21] in Table 4b. The FDPF increases above 10 MV due to pair production interactions in the metal.

The isocenter dose reduction in the presence of bilateral SS316L HPs ranged from 17 to 23%, and for Ti6Al4V, it ranged from 11 to 17%. For a unilateral HP, the respective dose reductions were 7%–19% and 3%–12%. This is shown in Table 5.

Five-field plan

This plan consisted of five equiangular spaced beams at gantry angles 54°, 126°, 198°, 270°, and 342°, with the 270° lateral beam intersecting the HP [Figure 7a].

The effect of various bilateral HPs on the DVH data for the PTV, bladder, and rectum at 6–20 MV using a 5F plan is shown in Figure 7a-d. The results are the same for unilateral prostheses as only one HP blocks the field for the 5F configuration.

An interesting observation for this beam configuration is that above 10 MV, increasing the beam energy does not cause a significant increase in the PTV dose, with $V_{95\%}$ increasing only from 80% to 92% from 10 MV to 20 MV for a SS316L HP.

Table 3: Back-scattered dose perturbation factors versus distance from the interface for (a) 6 MV, (b) 10 MV (c), 15 MV, and (d) 20 MV photon beams

a. 6 MV

P (mm)	SS316L	Ti6Al4V	UHMWPE
0	1.24	1.18	0.99
2	1.08	1.06	0.99
4	1.04	1.03	1.00
6	0.99	1.00	1.00

b. 10 MV

P (mm)	SS316L	Ti6Al4V	UHMWPE
0	1.27	1.20	0.99
3	1.10	1.05	0.99
6	1.02	1.02	1.00
9	1.00	1.00	1.00

c. 15 MV

P (mm)	SS316L	Ti6Al4V	UHMWPE
0	1.32	1.21	0.99
5	1.21	1.08	1.00
10	1.07	1.00	1.00
12	1.00	1.00	1.00

d. 20 MV

P (mm)	SS316L	Ti6Al4V	UHMWPE
0	1.38	1.25	1.00
5	1.25	1.13	0.99
10	1.08	1.00	0.99
15	1.00	1.00	1.00

SS316L: Stainless steel, Ti6Al4V: Titanium, P: Distance from interface UHMWPE: Ultra-high-molecular-weight polyethylene

Table 4: Forward dose perturbation factor calculated versus energy at the distal interface in (a) this study and (b) Reft *et al.*^[21]

a. FDPF at distal interface

Energy (MV)	SS316L	Ti6Al4V	UHMWPE
6	0.62	0.84	0.99
10	0.75	0.87	1.00
15	0.80	0.94	1.00
20	0.93	1.04	1.01

b. FDPF at distal interface

Energy (MV)	Bone	Steel	Lead
6	0.94	0.85	0.84
18	1.05	1.20	1.41

FDPF: Forward dose perturbation factor, SS316L: Stainless steel, Ti6Al4V: Titanium, UHMWPE: Ultra-high-molecular-weight polyethylene

This is a double increase in beam energy, though the PTV is still underdosed. The maximum rectal and bladder volume receiving at least 80% of the prescription dose is 17% and 27%, for SS316L and Ti6Al4V, respectively. The isocenter dose reduction in the presence of unilateral SS316 L HPs ranged 2%–14%, and for Ti6Al4V it ranged 1%–11%. This is shown in Table 6.

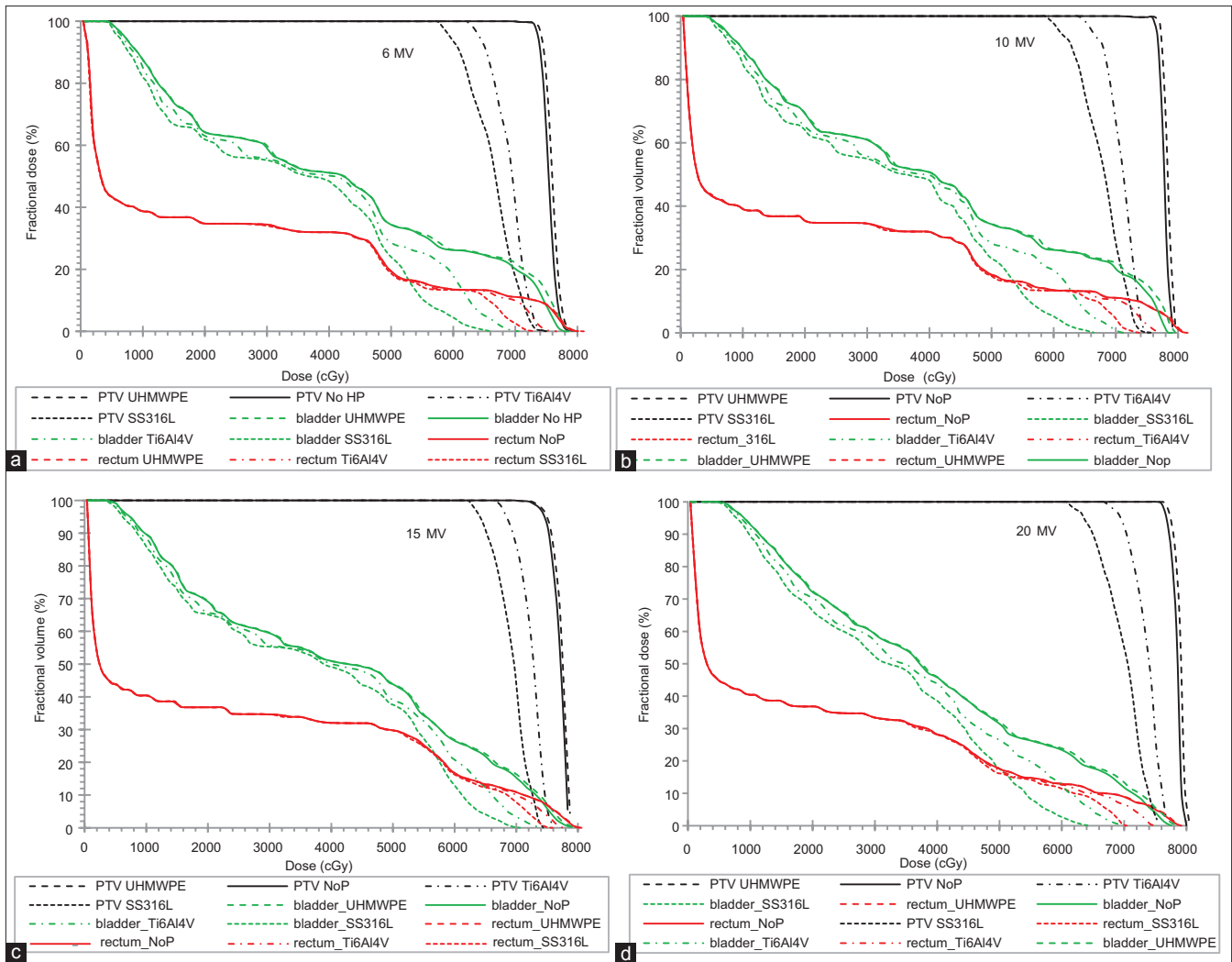


Figure 5: Comparison of the cumulative dose-volume histogram data of the planning target volume, bladder and rectum for various bilateral prostheses using a 4F equiangular plan for (a) 6 MV, (b) 10 MV, (c) 15 MV, and (d) 20 MV, NoP: No prostheses; SS316L: Stainless steel; Ti6Al4V: Titanium; UHMWPE: Ultra-high-molecular-weight polyethylene; PTV: Planning target volume

Simulation studies have shown that the dose for the bilateral HP case is within the statistical noise of the data and was not included.

Six-field plan

This plan was composed of 6 fields at gantry angles 45°, 90°, 135°, 225°, 270°, and 315°, i.e., two bilateral fields and two pairs of opposed oblique fields [Figure 8a]. The largest PTV underdosage in the presence of a unilateral SS316L and Ti6Al4V HP for this particular 6F plan is 27% and 4.5%, respectively. For bilateral HPs, it increases to 30% and 6.9%, respectively. Comparison of the cumulative DVH data of the PTV, bladder and rectum for various bHPs using a 6F plan for 6-20 MV is shown in Figure 8a-d.

From Table 7, the PTV dose reduction in the presence of a unilateral SS316L HP for the 6F plan is 10.3%, and for Ti6Al4V, it is 6.2% at 6 MV. At 20 MV, the dose reduction can be minimized to 1.0% for Ti6Al4V. No significant dose reduction

occurs for UHMWPE. The percentage dose reduction as a function of beam energy for the 6F plan is shown in Figure 9.

The rate of dose reduction for SS316L and Ti6Al4V alloys is more pronounced at lower photon energies. At higher beam energies (>15 MV), the rate of dose reduction diminishes over the energies studied here. The same trend was observed for the 4F and 5F plans, although in a 5F plan, the results would be the same between unilateral and bilateral prostheses.

Figure 10a and b shows the relationship between the number of beams and the target coverage for a patient fitted with bilateral titanium alloy at 6 and 15 MV. The 6F plan gives the best PTV coverage.

DISCUSSION

The MC simulation of a full linac head design and beam production for 6–20 MV X-ray beams was successfully performed, and the beam parameters were benchmarked against the machine’s

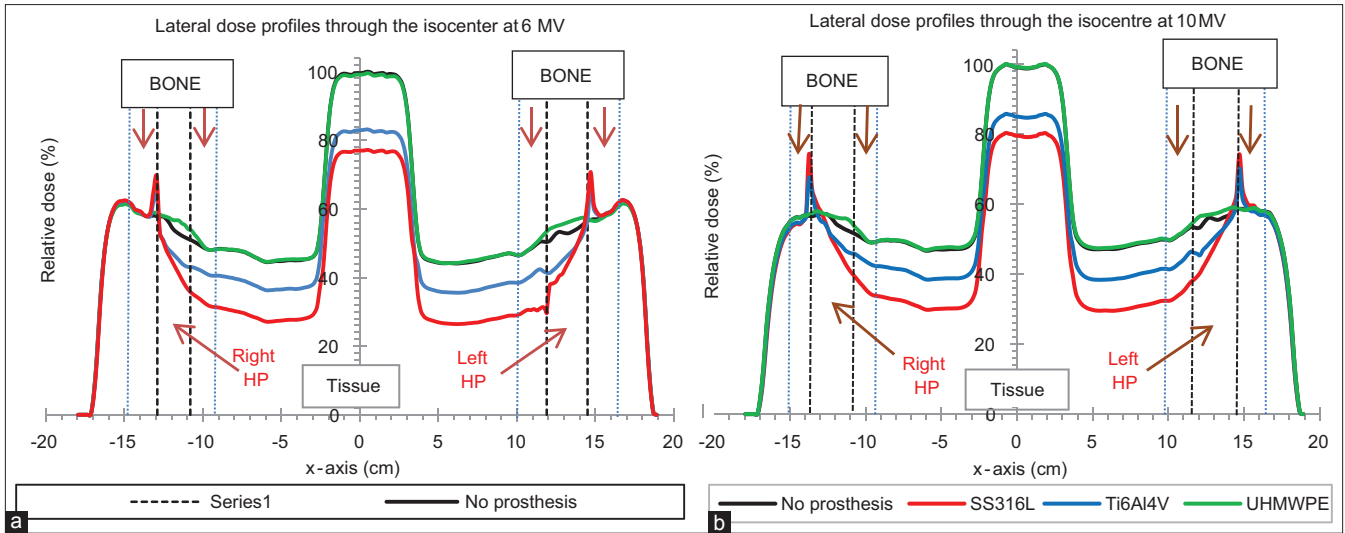


Figure 6: Comparisons of lateral dose profiles passing through the mid-prostheses on the central axial slice for a 4-field box at (a) 6 and (b) 10 MV. Interface regions are marked by broken lines

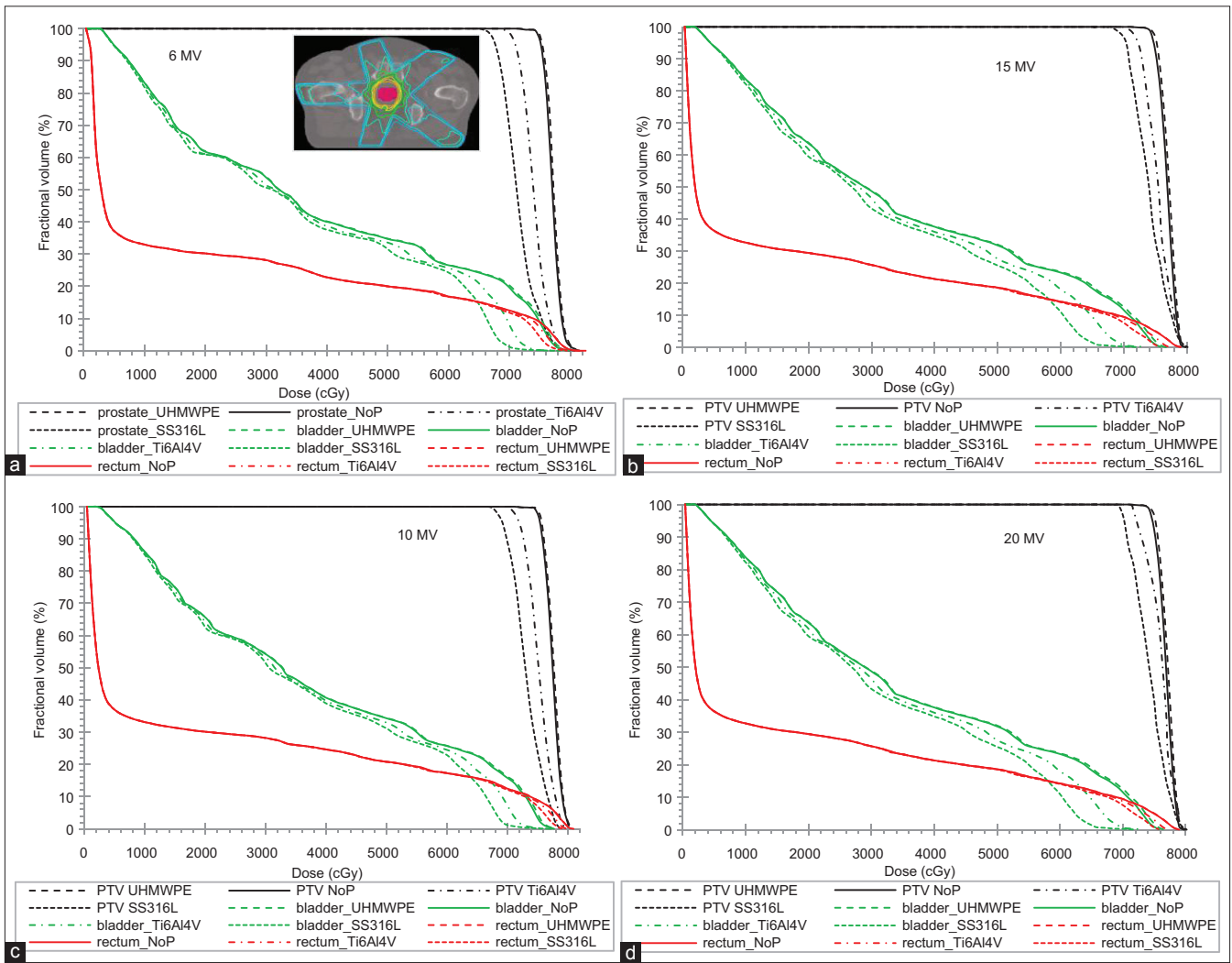


Figure 7: Comparison of the cumulative dose-volume histogram data of the planning target volume, bladder and rectum for various bilateral prostheses using a 5F equiangular plan for (a) 6 MV, (b) 10 MV, (c) 15 MV, and (d) 20 MV; NoP: No prostheses; SS316L: Stainless steel; Ti6Al4V: Titanium; UHMWPE: Ultra-high-molecular-weight polyethylene; PTV: Planning target volume

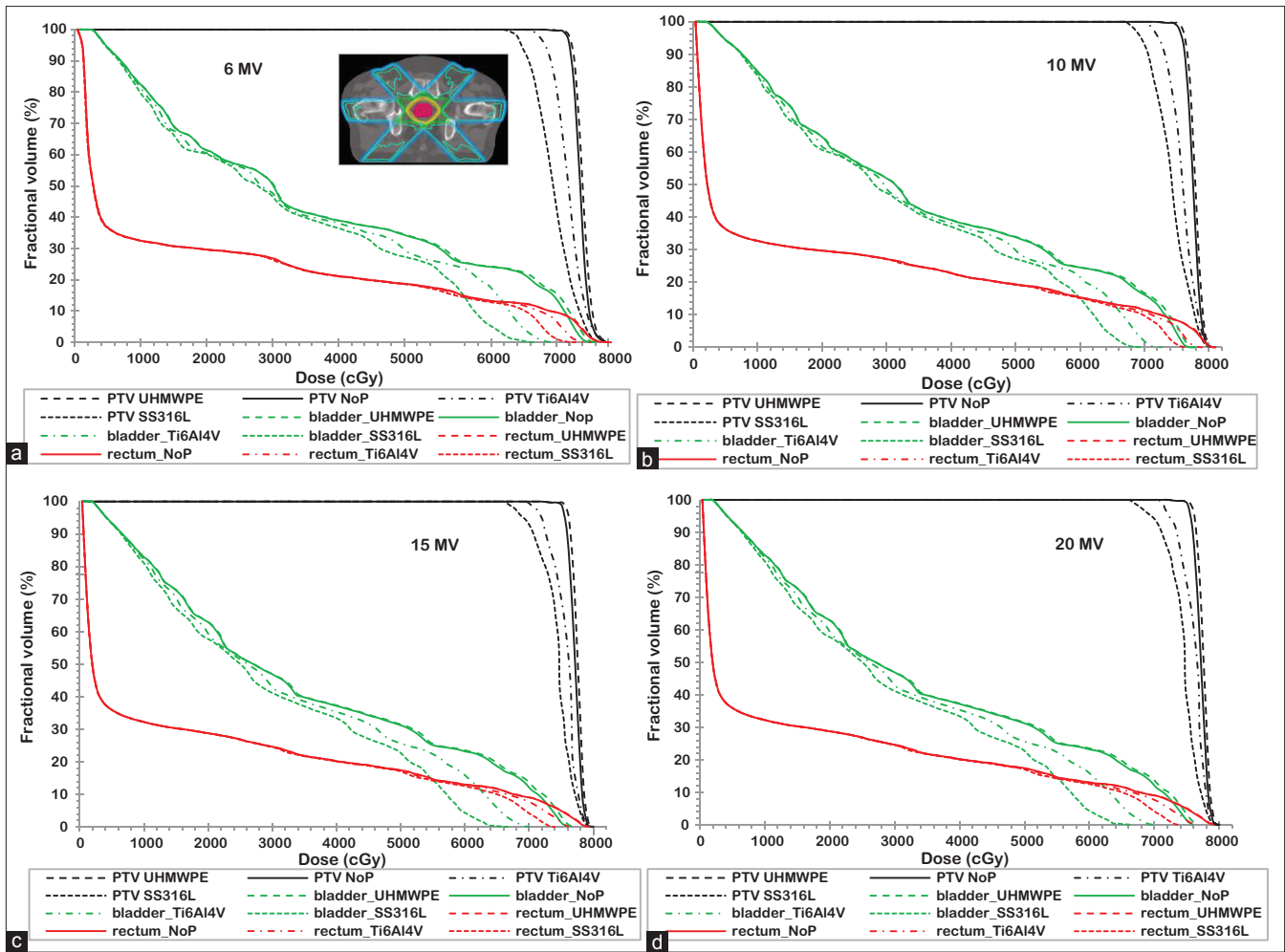


Figure 8: Comparison of the cumulative dose-volume histogram data of the planning target volume, bladder and rectum for various bilateral prostheses using a 6F equiangular plan for (a) 6 MV, (b) 10 MV, (c) 15 MV, and (d) 20 MV; NoP: No prostheses; SS316L: Stainless steel; Ti6Al4V: Titanium; UHMWPE: Ultra-high-molecular-weight polyethylene; PTV: Planning target volume

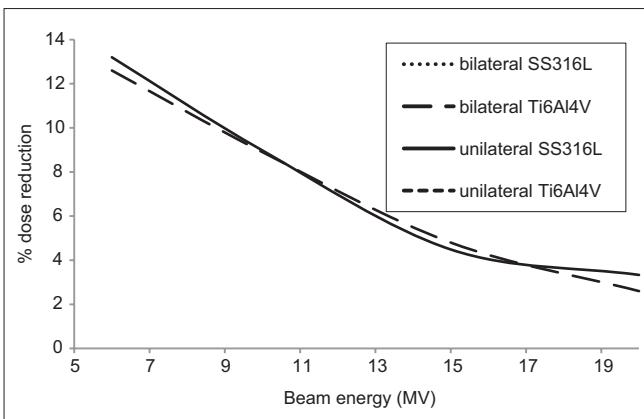


Figure 9: Percentage dose reduction as a function of beam energy in a 6F plan for a patient with unilateral and bilateral SS316L and Ti6Al4V hip prostheses

commissioning data. Beam parameter data were within 1% of measured data. For CT-based simulations, the dosimetric influence of HPs on the mid axial slice and in some volumes was evaluated

Table 5: Isocenter dose perturbation versus beam energy in a 4F box plan for (a) bilateral and (b) unilateral hip prostheses

a. Bilateral HPs			
Energy (MV)	Percentage dose reduction		Percentage dose increase
	SS316L	Ti6Al4V	UHMWPE
6	22.8	16.8	<1
10	20.4	14.8	<1
15	18.5	12.7	<1
20	16.9	10.6	<1
b. Unilateral HP			
Energy (MV)	Percentage dose reduction		Percentage dose increase
	SS316L	Ti6Al4V	UHMWPE
6	18.6	12.3	<1
10	15.1	9.5	<1
15	10.3	5.6	<1
20	6.8	2.5	<1

SS316L: Stainless steel, Ti6Al4V: Titanium, UHMWPE: Ultra-high-molecular-weight polyethylene

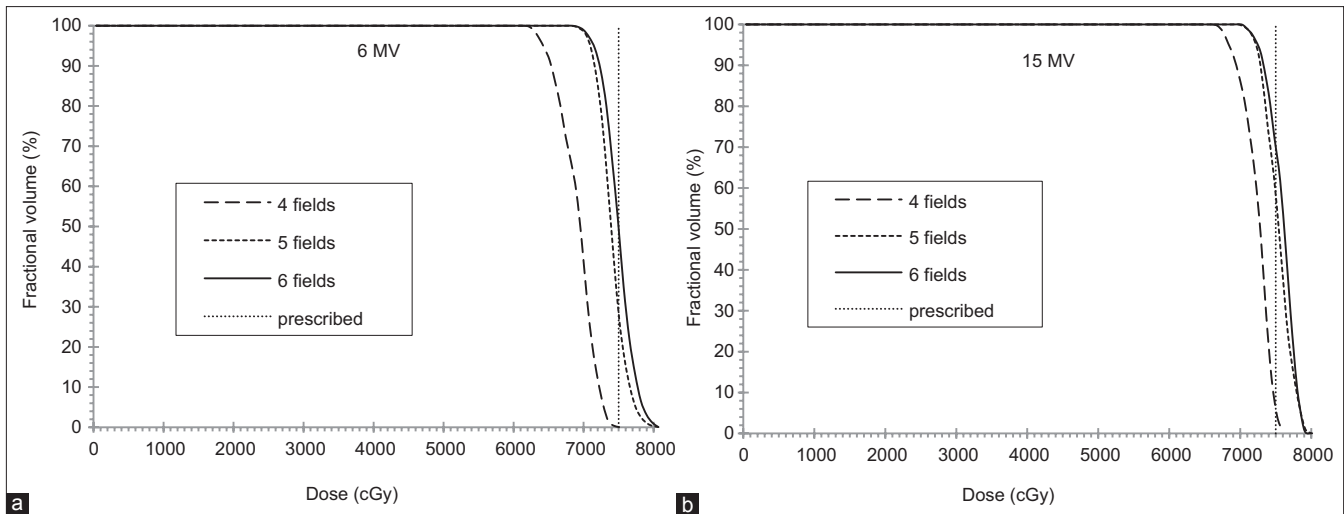


Figure 10: Dose-volume histogram data showing the relationship between the number of beams and the planning target volume coverage for (a) 6 MV and (b) 15 MV photon beams for the bilateral Ti6Al4V hip prosthesis case. More beams produce a better dose distribution

Table 6: Isocenter dose perturbation versus beam energy in a 5F plan for a patient with unilateral hip prostheses

Energy (MV)	Unilateral prostheses		
	Percentage dose reduction		Percentage dose increase
	SS316L	Ti6Al4V	UHMWPE
6	14.2	11.0	<1
10	9.6	7.5	<1
15	5.3	4.2	<1
20	2.3	1.1	<1

The dose reduction is exactly the same for the bilateral HP case. The data are within the statistical noise. HP: Hip prostheses, Ti6Al4V: Titanium, SS316L: Stainless steel, UHMWPE: Ultra-high-molecular-weight polyethylene

Table 7: Isocenter dose perturbation versus beam energy in a 6F plan for bilateral and unilateral hip prostheses

Energy (MV)	a. Bilateral HPs		
	Percentage dose reduction		Percentage dose increase
	SS316L	Ti6Al4V	UHMWPE
6	15.1	12.6	<1
10	10.1	8.9	<1
15	7.2	4.8	<1
20	4.0	2.6	<1
Energy (MV)	b. Unilateral HPs		
	Percentage dose reduction		Percentage dose increase
	SS316L	Ti6Al4V	UHMWPE
6	10.3	6.2	<1
10	6.9	4.2	<1
15	3.5	2.4	<1
20	2.1	1.0	<1

HP: Hip prostheses, Ti6Al4V: Titanium, SS316L: Stainless steel, UHMWPE: Ultra-high-molecular-weight polyethylene

by quantifying the radiation absorption and scatter in the shadow of the HP and on the interfaces. The target coverage was quantified by calculating $V_{95\%}$ values for each plan.

High-energy beams have greater penetrating power, hence the increased $V_{95\%}$ with energy. The dose to critical organs was independent of the beam energy used, or at least no general trend was noticeable. Although OAR dose reduction occurred when high-Z materials were used, OAR sparing was not the planning intent; therefore little can be said about OAR dose reduction.

For a 4F plan, the dependence of dose distribution on beam energy at the isocenter was weak, except close to the prosthesis as also reported by Erlanson *et al.*^[32] in a similar study. They also found ~25% dose enhancement at the proximal interface, extending up to 2 cm from the interface at 50 MV.

Increasing the number of beam portals generally improves the plan quality. The 5F plan causes a smaller PTV dose reduction compared to a 4F box since only one beam intersects a HP which is about 20% of the dose delivered by 5 equally weighted fields, while the 4F field box has 2/4 fields (50%) intersecting the prostheses. The small impact with regard to beam energy is because five fields of equal weights are used to deliver dose to the PTV and only one passes through the HP at 270°. The 6F plan produces an even better PTV dose conformity and less dose perturbation compared to the 4F box. This is because the 6F plan has 2/6 fields (33%) passing through the HPs compared to 50% in a 4F plan. The 5F plan has 20% of its fields intersecting the HP while the 6F plan has only 1/6 (17%) intersecting the HP; hence, the 6F plan has less dose perturbation for a unilateral HP. However, for bilateral HPs, the 6F plan has 33% of its beams intersecting HPs compared to 20% in a 5F plan, and therefore the dose perturbation would be worse for a 6F plan. Results highlight the influence of the implant’s composition, the beam energy, and position relative to the HP on the dose distribution.

One approach to correct for the effect of HP is to use special beam arrangements (even noncoplanar beam arrangements) that completely or partially avoid the prosthesis. Reducing the weight of beams intersecting the prosthesis or increasing their monitor units (MUs) to account for prosthesis attenuation may provide an acceptable plan. An understanding of the dose perturbation effect of HPs allows greater exploitation of gantry angles, number of beam portals, etc., and potentially improves dosimetric conformality. UHMWPE poses negligible dose perturbation and therefore does not need any MU compensation. It was to be expected that there would be more dispersion in the results for SS316L materials than for the UHMWPE, simply because of the differences in the atomic number. However, the cause of the inconsistency in the results at this point has not yet been understood.

This study confirms the results in similar studies; the advantage being the exclusion of imaging artifacts since heterogeneous media could be introduced into the CT-phantom in a synthetic way. This work may also have applicability to patients with other pelvic malignancies. However, given the patient size variation and the prostate-to-prostheses relationship, no general information can be gleaned, since one patient anatomy was investigated. The work can nevertheless be repeated on a representative number of patient samples. Also, the study is restricted to 3DCRT which might limit its relevance to IMRT and VMAT dominated environments. These techniques are, however, difficult to implement in MC simulations.

Financial support and sponsorship

This research and the publication thereof is the result of funding provided by the South African Medical Research Council (MRC) in terms of MRC's Flagship Awards Project SAMRC-RFA-UFSP-01-2013/HARD with funds from the National Treasury under its Economic Competitiveness and Support Package.

Conflicts of interest

There are no conflicts of interest.

REFERENCES

- Agapito J. Radical radiation therapy for carcinoma of the prostate in patients with a single hip prosthesis: A technique analysis using dose-volume histograms. *Med Dosim* 2001;26:243-50.
- Su A, Reft C, Rash C, Price J, Jani AB. A case study of radiotherapy planning for a bilateral metal hip prosthesis prostate cancer patient. *Med Dosim* 2005;30:169-75.
- Martin DA, Hruby G, Whitaker MK, Foo KY. Constrained-beam inverse planning for intensity-modulated radiation therapy of prostate cancer patients with bilateral hip prostheses. *J Med Imaging Radiat Oncol* 2012;56:703-7.
- Rana SB, Pokharel S. A dosimetric study of volumetric modulated arc therapy planning techniques for treatment of low-risk prostate cancer in patients with bilateral hip prostheses. *South Asian J Cancer* 2014;3:18-21.
- Morin RL, Raeside DE. Removal of streaking artifact in computed tomography. *J Med Syst* 1982;6:387-97.
- Wang G, Snyder DL, O'Sullivan JA, Vannier MW. Iterative deblurring for CT metal artifact reduction. *IEEE Trans Med Imaging* 1996;15:657-64.
- Robertson DD, Yuan J, Wang G, Vannier MW. Total hip prosthesis metal-artifact suppression using iterative deblurring reconstruction. *J Comput Assist Tomogr* 1997;21:293-8.
- Rosewall T, Kong V, Vesprini D, Catton C, Chung P, Ménard C, *et al.* Prostate delineation using CT and MRI for radiotherapy patients with bilateral hip prostheses. *Radiother Oncol* 2009;90:325-30.
- Brook OR, Gourtsoyianni S, Brook A, Mahadevan A, Wilcox C, Raptopoulos V, *et al.* Spectral CT with metal artifacts reduction software for improvement of tumor visibility in the vicinity of gold fiducial markers. *Radiology* 2012;263:696-705.
- Boas FE, Fleischmann D. Computed tomography artifacts: Causes and reduction technique. *Imaging Med* 2012;4:22940.
- Axente M, Paidi A, Von Eyben R, Zeng C, Bani-Hashemi A, Krauss A, *et al.* Clinical evaluation of the iterative metal artifact reduction algorithm for CT simulation in radiotherapy. *Med Phys* 2015;42:1170-83.
- Meyer E, Raupach R, Lell M, Schmidt B, Kachelriess M. Normalized metal artifact reduction (NMAR) in computed tomography. *Med Phys* 2010;37:5482-93.
- Buzug T, Oehler M. Statistical image reconstruction for inconsistent CT projection data. *Methods Inf Med* 2007;46:261-9.
- Lemmens C, Faul D, Nuyts J. Suppression of metal artifacts in CT using a reconstruction procedure that combines MAP and projection completion. *IEEE Trans Med Imaging* 2009;28:250-60.
- Boas FE, Fleischmann D. Evaluation of two iterative techniques for reducing metal artifacts in computed tomography. *Radiology* 2011;259:894-902.
- Khan FM, Potish RA. *Treatment Planning in Radiation Oncology*. Baltimore: William and Wilkins; 1998.
- Lin SY, Chu TC, Lin JP, Liu MT. The effect of a metal hip prosthesis on the radiation dose in therapeutic photon beam irradiations. *Appl Radiat Isot* 2002;57:17-23.
- Eng TY. Dose attenuation through a titanium alloy hip prosthesis. *Med Dosim* 2000;25:7-8.
- Prabhakar R, Kumar M, Cheruliyil S, Jayakumar S, Balasubramanian S, Cramb J. Volumetric modulated arc therapy for prostate cancer patients with hip prosthesis. *Rep Pract Oncol Radiother* 2013;18:209-13.
- Kung JH, Reft H, Jackson W, Abdalla I. Intensity-modulated radiotherapy for a prostate patient with a metal prosthesis. *Med Dosim* 2001;26:305-8.
- Reft C, Alecu R, Das JJ, Gerbi BJ, Keall P, Lief E, *et al.* Dosimetric considerations for patients with HIP prostheses undergoing pelvic irradiation. Report of the AAPM Radiation Therapy Committee Task Group 63. *Med Phys* 2003;30:1162-82.
- Carolan M, Dao P, Fox C, Metcalfe P. Effect of hip prostheses on radiotherapy dose. *Australas Radiol* 2000;44:290-5.
- Buffard E, Gschwind R, Makovicka L, David C. Monte Carlo calculations of the impact of a hip prosthesis on the dose distribution. *Nucl Instrum Methods Phys Res B* 2006;251:9-18.
- Rogers DW, Walters B, Kawrakow I. *BEAMnrc User's Manual NRC Report PIRS 509 (a) RevH. Ionizing Radiation Standards*; 2004.
- Rogers DW, Faddegon BA, Ding GX, Ma CM, We J, Mackie TR. BEAM: A Monte Carlo code to simulate radiotherapy treatment units. *Med Phys* 1995;22:503-24.
- Ding GX, Yu CW. A study on beams passing through hip prosthesis for pelvic radiation treatment. *Int J Radiat Oncol Biol Phys* 2001;51:1167-75.
- Walters B, Kawrakow I, Rogers DW. *DOSXYZnrc User's Manual. Ionizing Radiation Standards. National Research Council of Canada, Ottawa, NRC Report PIRS-794*; 2005.
- Alvarado J, Maldonado R, Marxuach J, Otero R. Biomechanics of hip and knee prostheses. *Appl Eng Mech Med* 2003:6-22.
- Zhan L, Jiang R, Osei EK. Beam coordinate transformations from DICOM to DOSXYZnrc. *Phys Med Biol* 2012;57:N513-23.
- Chetty IJ, Curran B, Cygler JE, DeMarco JJ, Ezzell G, Faddegon BA, *et al.* Report of the AAPM Task Group no 105: Issues associated with

- clinical implementation of Monte Carlo-based photon and electron external beam treatment planning. *Med Phys* 2007;34:4818-53.
31. Landberg T, Chavaudra J, Dobbs HJ, Hanks G, Johansson KA, Mller T, *et al.* Prescribing Recording and Reporting Photon Beam Therapy. ICRU Report 50. ICRU, Bethesda, Maryland; 1993.
 32. Erlanson M, Franzén L, Henriksson R, Littbrand B, Löfroth PO. Planning of radiotherapy for patients with hip prosthesis. *Int J Radiat Oncol Biol Phys* 1991;20:1093-8.